CFD simulation of a 10 kW chemical looping with oxygen uncoupling system: effects of process and fuel parameters

Matthew A. Hamilton[1*#], Kevin J. Whitty[1], JoAnn S. Lighty[1]

[1] *University of Utah, 50 S. Central Campus Dr. Rm 3290, Salt Lake City, UT, USA*

**Corresponding Author, Matthew.A.Hamilton@utah.edu, [#]Presenting Author*

Abstract – Chemical looping with oxygen uncoupling (CLOU) is a carbon-capture technology that utilizes a metal oxide as an oxygen carrier to separate oxygen from air. The metal oxide is oxidized in an air reactor and releases gaseous oxygen in a fuel reactor where a fuel, such as coal, is fed. CFD simulations will expedite the scale-up of CLOU systems to demonstration and utility size plants by resolving technical concerns and showing the CLOU technology at larger scales. In this study, Barracuda was used as the platform for simulation. The CLOU kinetics were incorporated into the simulation and the coal kinetics were explored for one-step versus two-step combustion kinetics. Two cases were run, one for a pure carbon-char and one with the inclusion of ash. Using the two-step kinetics and inclusion of ash in the simulation yielded reasonable temperatures in both the gas and particle phases. Also studied were the effects of heat input, via increasing the coal feed, and coal particle diameter. These simulations showed that the increasing of the coal heat input had little effect as compared to changing the particle diameter. Increased particle diameter increased the particle temperatures and decreased the carbon capture efficiency.

1 Introduction

Carbon dioxide emissions have been the largest contributor to climate forcing, with one of the largest source coming from the combustion of fossil fuels for the generation of electricity. These methods for electricity generation are expected to be a dominate source until 2030 [1–3]. To minimize and potentially eliminate the carbon dioxide emissions, carbon capture technologies have been explored. Scrubbing the combustion products with different sorbents has been shown to be successful as well as using an oxycombustion process. These processes have shown energy penalties of 7-9% and 5-8% respectively [4,5]. Chemical looping combustion (CLC) is a novel technology for inherent separation of O_2 from air utilizing a reversible oxidation/reduction of metals. In the air reactor, the metal is oxidized with air to form a metal oxide. This metal is then transferred to a reactor where it is reduced with a gaseous fuel. The metal is then returned to the first reactor, completing the loop. Chemical looping with oxygen uncoupling (CLOU) is a subset of CLC where the metal in the fuel reactor releases gaseous oxygen that can be used to burn solid fuels. CLOU's distinct advantage over CLC is the elimination of the need to change solid fuels into gaseous phase products though the gasification reaction, but only a few materials including copper show CLOU properties [6–8].

In copper-based CLOU, the copper oxygen carrier particles are oxidized in the air reactor (AR) to cupric oxide (CuO) and then transferred to the fuel reactor (FR), where the coal is introduced. In the FR cupric oxide reduces forming cuprous oxide (Cu_2O) particles and releasing O_2. The released O_2 reacts directly with the coal to form CO_2 and H_2O, are 50x faster reactions as compared to the gasification reaction [8–11]. CLC and CLOU systems have been operated up to 1 MW in heat release [12,13]. Chemical looping scale-up has had little research due to current technical challenges and the cost of manufacturing the system.

Computational fluid dynamic (CFD) simulations have been shown to aid in scale-up and lead to improvement in unit operations. Due to the complicated nature of particle-fluid interactions and the computational expense associated with these CFD codes little work has been done until recent years in CLC and CLOU [14–18]. Some of these simulations have included the Eulerian-Lagrangian (E-L) multiphase-particle in cell (MP-PIC) method. The MP-PIC method is the basis for the Barracuda VR® code. The full details can be found in Andrew et al. [19]. The MP-PIC method solves the continuous fluid phase with the full mass and momentum equations. A Liouville equation is used to solve the particle phase to obtain the position, velocity and size distribution of particles. The inclusion of particle clouds has been used in the MP-PIC method to increase the number of real particles that can be tracked. Further developments of the MP-PIC method have been completed by Snider and O'Rourke [20–23]. The code has been used to simulation NETL's CLC simulation by Parker [17]. Peltola et al. showed CLOU kinetics in a CFD simulation [24]. Recently, Hamilton et al. have shown CLOU kinetics in a 10 kW system [25]; however, only a one-step char combustion process was included and particle and gas temperatures were shown to be excessively high, above ash fusion temperatures.

This study has three major objectives: first, investigate the effects of coal particle diameter and heat input on the system; second, exam the effects of one-step and two-step combustion mechanisms; and, third show the effects of ash in the char on the particle temperatures.

2 Computational Methods

2.1 Chemical Reactions and Cases

The chemical kinetics of copper-based CLOU include the oxidation of cuprous oxide, reduction of cupric oxide, and reactions involving the coal material. In Barracuda-VR® chemical reactions can be run as a volume average rate, r ($mol \cdot s^{-1}m^{-3}$ or $kg \cdot s^{-1}m^{-3}$), or discrete particle kinetics, r_p ($kg \cdot s^{-1}$). There are several advantages for each. The volume average rate has less computational expense resulting in faster simulations and has been shown to be robust. There are several disadvantages for using the volume average rate. The temperature used is the bulk gas temperature which can be lower than the particle surface temperature resulting in reactions that are slower than what they actually are [23]. Discrete particle reactions are recommend by CPFD for most heterogeneous reactions [26]. The discrete particle reaction uses individual particle clouds that are not averaged over the cell. These results are more accurate with multiple types of particles participating in reactions in the same cell, i.e. the fuel reactor contains both decomposition of cupric oxide and the combustion of coal char.

The experimental details and developed experimental rates for the copper oxide reactions are found in Sahir et al. and Clayton et al. [11,27]. The details of converting from the experimental rates to the simulation inputs can be found in Hamilton et al. [25]. The copper oxide reaction rates, Reaction 1 and 2, can be found in Table 1. The study in Hamilton et al. used a one-step char combustion model, Reaction 3. The two-step model, where the heterogeneous reaction of char and oxygen form carbon monoxide and the carbon monoxide subsequently reacts homogenously with oxygen to form carbon dioxide, is Reaction 4 in Table 1 and the volume average rate is Reaction 1 in Table 2.

Table 1: Discrete particle reaction rates used for heterogeneous reactions

Number	Reaction	Discrete Particle Reaction Rate	Case	Source
1	$Cu_2O(s) + O_2 \rightarrow CuO$	$\frac{dm_{Cu_2O}}{dt} = 1.13 \times 10^{10} m_{CuO} \theta_f \exp\left(-\frac{41{,}500}{T}\right) - 5600 m_{CuO} \theta_f \exp\left(-\frac{8180}{T}\right) p_{O_2}^{1.3}$	All	[25,27]
2	$CuO(s) \rightarrow Cu_2O + O_2$	$\frac{dm_{CuO}}{dt} = 3 m_{CuO} \theta_f \exp\left(-\frac{2350}{T}\right) p_{O_2} - 1.62 \times 10^8 m_{CuO} \theta_f \exp\left(-\frac{27{,}950}{T}\right)$	All	[11,25]
3	$C(s) + O_2 \rightarrow CO_2$	$\frac{dm_c}{dt} = -145{,}000 A_p \theta_f \cdot \exp\left(\frac{10{,}050}{T}\right) P_{O_2}$	1	[25,28]
4	$C(s) + ½\ O_2 \rightarrow CO$	$\frac{dm_c}{dt} = -145{,}000 A_p \theta_f \cdot \exp\left(\frac{10{,}050}{T}\right) P_{O_2}$	2, 3	[28]

Table 2: Volume average reaction rate used for homogenous reactions

Number	Reaction	Volume Average Reaction Rate	Case	Source
1	$CO + ½\ O_2 \rightarrow CO_2$	$r = -1.4 \times 10^9 \exp\left(-\frac{13{,}600}{T}\right) [CO][O_2]^{0.5}$	2, 3	[29,30]

The initial one-step char combustion kinetics are simple and allow for fast simulations. On the other hand, the two-step char combustion kinetics distribute the enthalpy of reaction across two reactions, with one reaction occurring in the gaseous phase. This should allow for more realistic particle temperatures. Table 3 lists the case for each of these reactions. Another case investigates the inclusion of ash constituents in the coal particle versus strictly carbon; the ash works as a particle heat sink. A summary of these studies can be found in Table 3.

Table 3: Summary of studies performed

Case Name (#)	Char Combustion Kinetics	Inclusion of Ash
One-Step (1)	One–step to carbon dioxide	No
Two-Step (2)	Two–step to carbon dioxide through carbon monoxide	No
Detailed Char (3)	Two–step to carbon dioxide through carbon monoxide	Yes

2.2 Particle Parameters

The oxygen carrier particles studied are cupric/cuprous oxide on silicon oxide (quartz). A fully oxidized particle contains 40% by mass cupric oxide with the remainder silicon oxide. Fully reduced particles are 37.3% by mass cuprous oxide with the remainder silicon oxide. The change in weight is due to the change in molecular weight from oxidized to reduced copper. The density of the particles is approximately 3150 kg m^{-3}. The detailed copper properties and thermodynamic parameters of copper oxide oxygen carrier can be found in the previous work of Hamilton et al. [25]. The coal char has a density of 2000 kg m^{-3}. Three coal particle size distributions were studied, while the oxygen carrier particle size distribution was held constant through all studies (Figure 1).

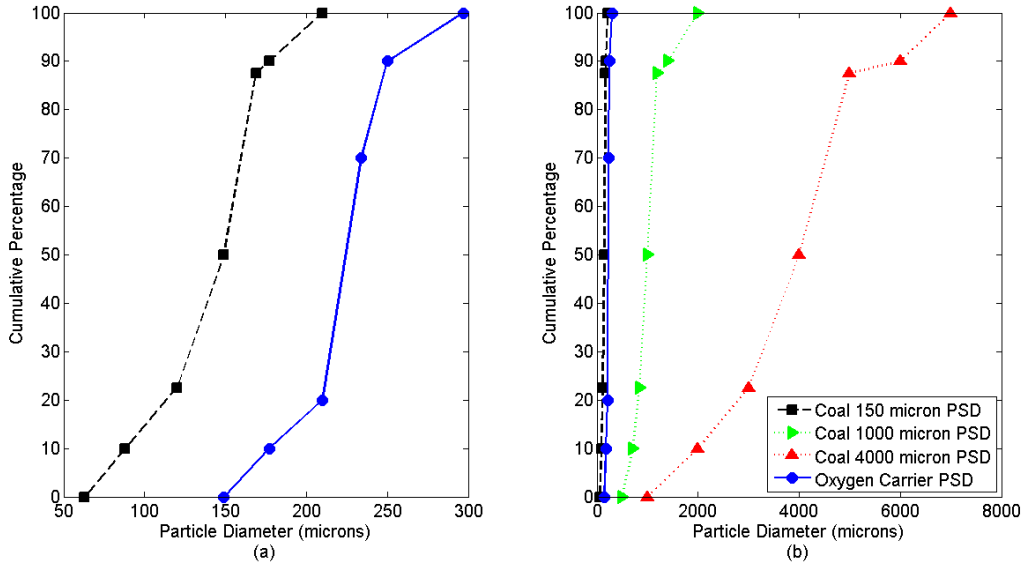

Figure 1: The PSDs of the particles in the system. (a) the oxygen carrier and 150-micron coal average, zoomed in; (b) all four distributions.

The ultimate analysis of the coal can be found in Table 4. The top five components of the ash are shown in Table 5. Barracuda VR® built in thermodynamic properties were used for the calcium oxide and experimental data can be found in Bodryakov and Morrell [31,32]; the data in these studies were used to generate the equations for thermal conductivity and specific heat seen in Equations 1 and 2, respectively.

$$k(T) = 27.2 - 0.0429T + 3.12 \times 10^{-5}T^2 - 7.43 \times 10^{-9}T^3 \quad (1)$$

$$c_p(T) = \begin{cases} 236 + 2.79T - 0.004T^2 + 3.2 \times 10^{-6}T^3 - 8.56 \times 10^{-10}T^4, T < 1000\ K \\ 873 + 0.04T + 6.4 \times 10^{-5}T^2 - 4.2 \times 10^{-8}T^3 + 8.8 \times 10^{-12}T^4, T \geq 1000\ K \end{cases} \quad (2)$$

where k is thermal conductivity, T is temperature, and c_p is specific heat. Particles start at 950 °C and there is a distribution of oxidation states: approximately 50% in the air reactor; 75% in the upper loop seal; 25% in the loop seal; and, a mixture in the fuel reactor.

Table 4: Ultimate analysis of coal based on case

Component	One-step and two-step	Detailed char
Carbon	100	88.7
Ash	-	11.3

Table 5: Ash components used in ash studies

Component	Percentage
SiO_2	43.3
Al_2O_3	19.6
CaO	23.9
Fe_2O_3	7.4
MgO	5.8

2.3 Reactor Modeled and Initial Conditions

The system simulated is a 10 kW bench-scale dual bubbling bed reactor located at the University of Utah (Figure 2). For both reactors all particles enter at the base of the reactor and flow up exiting at the top of the reactor. The air reactor narrows to a transport riser. In the design the bottom portion of the reactor can function in a bubbling bed regime and for this same flow the transport section is in a transport regime. The fuel reactor has an overflow pipe that runs up the center of the reactor. As particles enter the reactor the particles on the top of the dense bed fall through the overflow pipe. More details of the reactor set up can be found in Larsén [33].

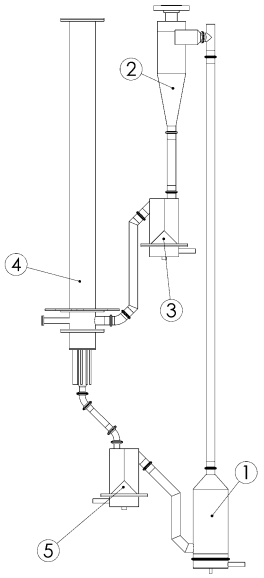

Figure 2: Schematic of the bench scale unit. (1) Air reactor, (2) cyclone, (3) upper loopseal, (4) fuel reactor, (5) lower loopseal.

In the system, the oxygen carrier particles enter one side of the fuel reactor and the fuel is introduced on the other side of the system through a screw feeder. The flowrates, species, and temperatures of the fluidizing gases are found in Table 6.

Table 6: Flowrates of major fluidizing gas

Location	Velocity [m·s^{-1}]	Gas species	Temperature [°C]
Air reactor inlet	0.24	Air	225
Fuel reactor inlet	0.018	Steam	300
Upper loopseal	0.028	Air (95% N_2 & 5% O_2)	950
Lower loopseal	0.018	Steam	525
Coal feed	$5 \cdot 10^{-5}$	Steam	300

2.4 Data analysis

The carbon capture efficiency is the ratio of gaseous phase carbon leaving the fuel reactor over the gaseous phase carbon leaving the system. This is shown in Equation 3.

$$\eta_{CC} = \left(\frac{F_{CO_2,FR} + F_{CO,FR}}{F_{CO_2,FR} + F_{CO,FR} + F_{CO_2,AR} + F_{CO,AR}} \right) \quad (3)$$

where $F_{i,j}$ is the flowrate of species i out of reactor j [9,34]. In case one, all terms containing carbon monoxide are eliminated.

3 Results and Discussion

3.1 Carbon Capture Efficiency

The effect of coal heat input on the carbon capture efficiency can be found in Figure 3. In this case, the coal particles had a PSD with an average of 150 micron, see Figure 1. From all three figures it can be determined that the heat input had very little effect on carbon capture efficiency. All cases and heat inputs were above the DOE target of 0.9 carbon capture efficiency. These particles are about 0.6 times the size of the oxygen carrier and density of the oxygen carrier. The smaller diameter coal particles a tendency to float on the bed and, after burning to sizes around 100 microns, entered the dilute phase of the bubbling bed.

Figure 4 shows the effect of the coal particle diameter on the carbon capture efficiency. The 4000-micron average diameter PSD coal particles, see Figure 1, had a carbon capture efficiency that was below the 0.9 DOE target; all other cases were above. These particles are 20 times the size of the oxygen carrier, but still about 0.6 the density of the oxygen carrier. The 4000 micron particles did not float on top of the bed until some combustion occurred and the particles shrank. The 1000-micron average diameter PSD case did not converge for the one-step combustion and two-step combustion. The char detailed with ash case for the 1000-micron average diameter PSD run did converge. This shows that including the ash content in the particles, which acts as a heat sink, improved the reliability of the simulations. The carbon capture efficiency for this run was also above the 0.9 DOE target.

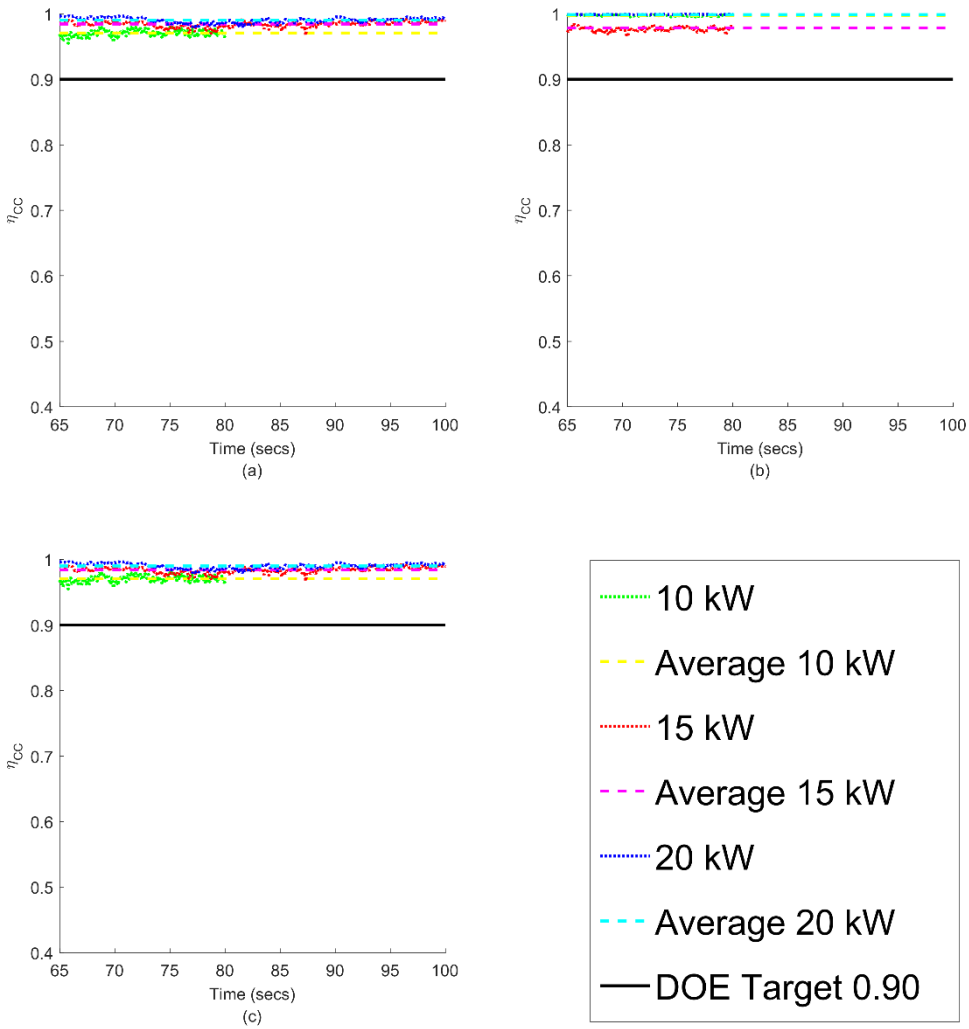

Figure 3: Effect of coal feed rate (as heat input) on carbon capture efficiency (a) one-step combustion (b) two-step combustion (c) detailed coal char with ash

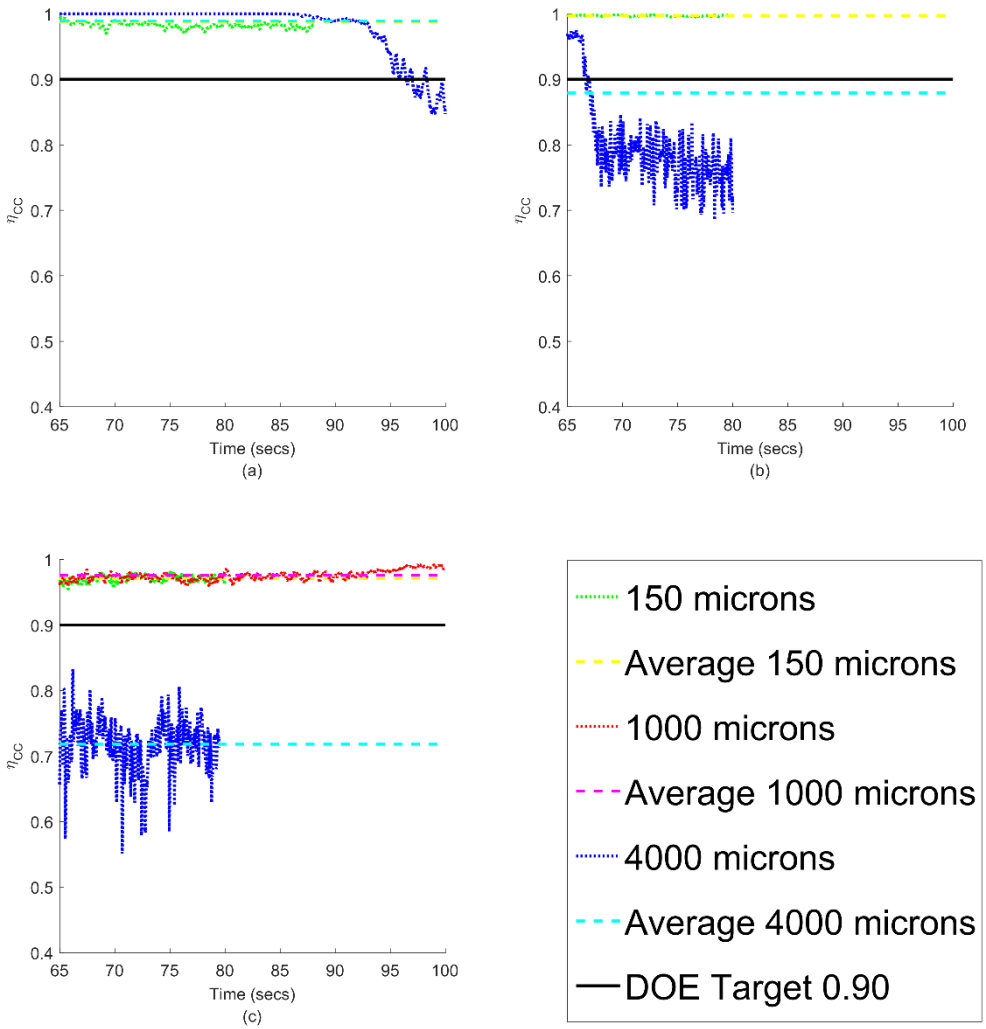

Figure 4: Effect of particle size on carbon capture efficiency a) one-step combustion (b) two-step combustion (c) detailed coal char with ash

3.2 Gas Concentrations in Reactors

The air reactor showed similar oxygen and carbon dioxide mole fractions for all cases and runs and the reactions all occurred in the bubbling bed portion of the air reactor. The effects of coal heat input on the fuel reactor oxygen concentration can be seen in Figure 5. The one-step and two-step combustion kinetics had similar profiles for the 10 kW and 15 kW coal heat input. These profiles start with the mole fraction around 0.05 which is the equilibrium mole fraction at 950 °C. This mole fraction increased through the dense bed to a max just above 0.06, with a corresponding increase in the bed temperature. The concentration then dropped at the top of the dense bed and decreased through the dilute phase. The decrease in the oxygen in the dilute phase was due to a low concentration of oxygen carrier particles releasing oxygen and a higher concentration of coal char in this phase, as compared with the dilute phase, resulting in oxygen consumption.

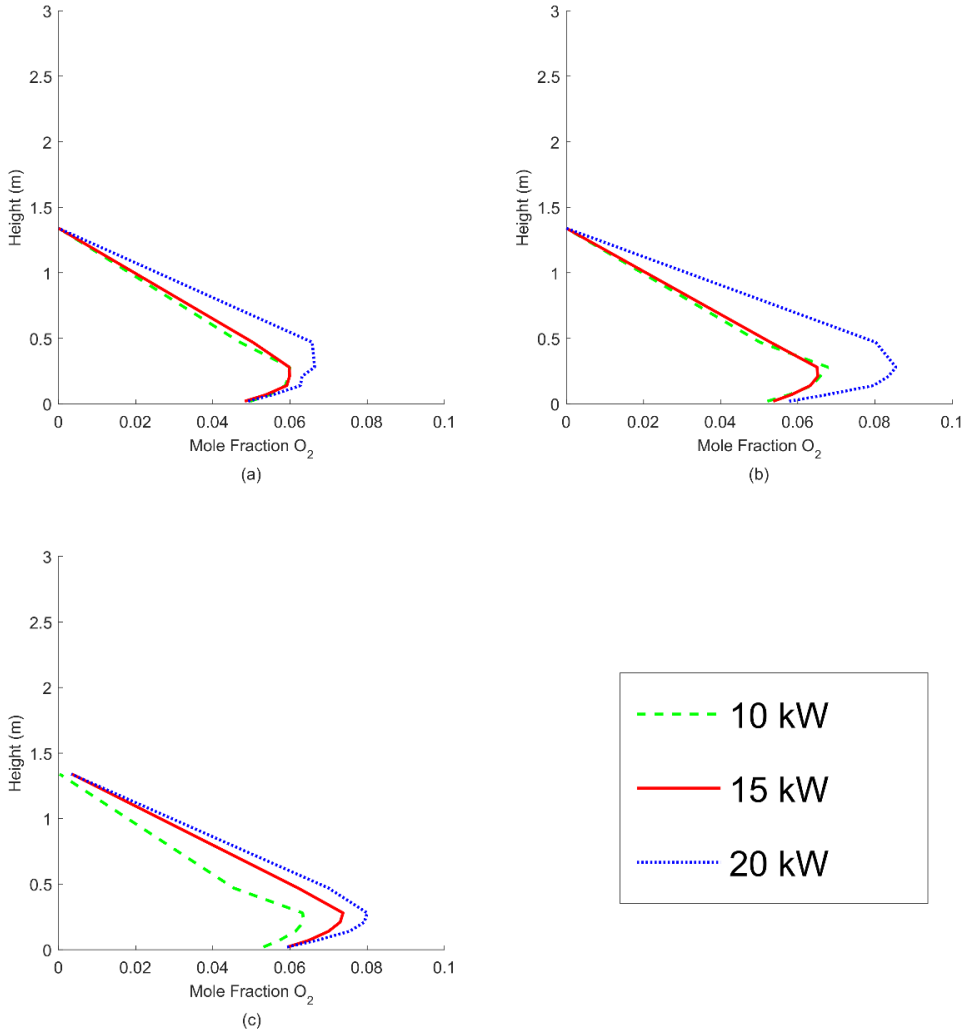

Figure 5: The effect of heat input on fuel reactor average oxygen concentration for (a) one-step combustion (b) two-step combustion (c) detailed coal char with ash.

The effects of coal particle diameter on the fuel reactor oxygen concentration can be seen in Figure 6. The 150-micron average diameter PSD runs are the same as the 10 kW runs in Figure 5. The oxygen concentration for the 4000-micron average diameter PSD case was similar in all three cases with the oxygen mole fraction staying about at 0.05 due to the more uniform temperature of the gas temperature. The 1000-micron average diameter PSD, detailed char case showed an increase in oxygen mole fraction through the dense phase similar to what occurred in the 150-micron average diameter PSD run, but, after the dense phase, the concentration stayed constant through the dilute phase.

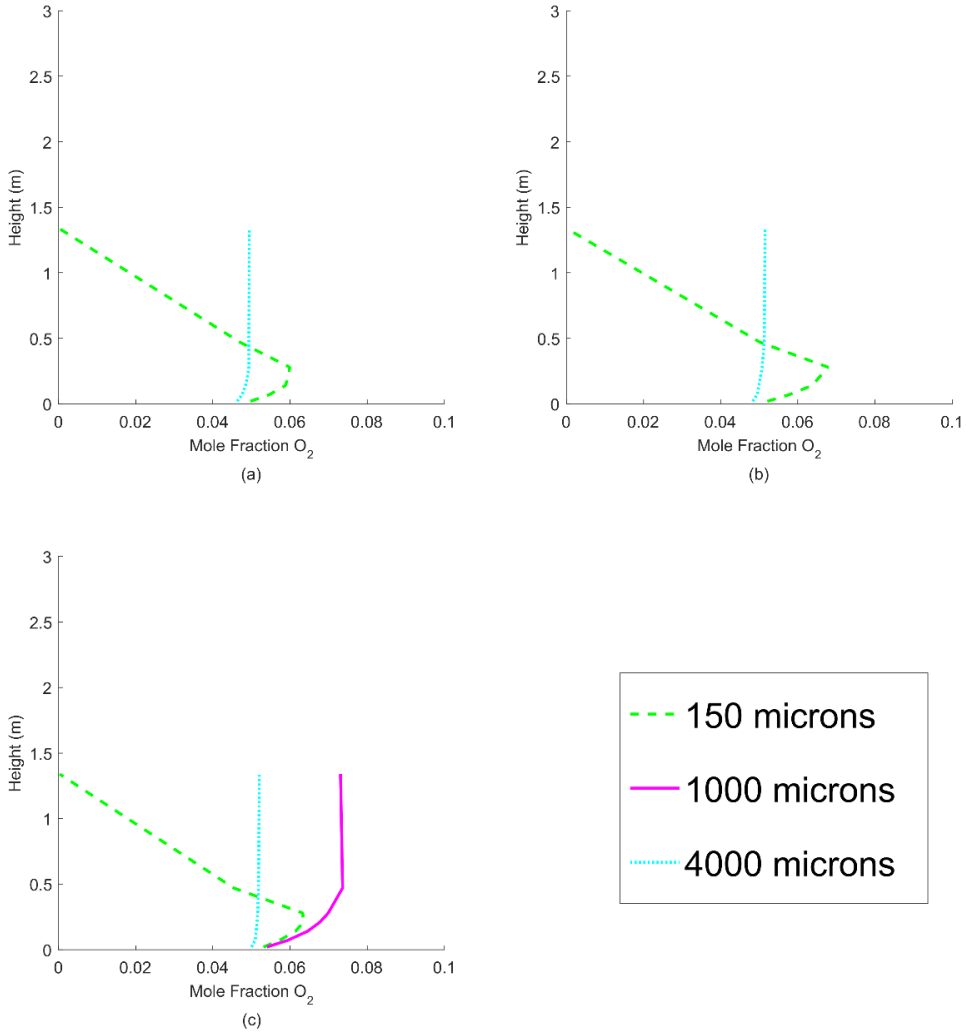

Figure 6: Fuel reactor average oxygen concentration vs. height effect of coal char particle diameter (a) one-step combustion (b) two-step combustion (c) detailed coal char with ash

Figure 7 shows the effect of coal particle diameter on the carbon dioxide mole fraction. This figure shows that the 4000-micron average diameter PSD runs had a lower mole fraction of carbon dioxide, most likely is due to slower reaction. The 1000-micron average diameter PSD run closely followed the 150-micron average diameter PSD runs. These runs resulted in the carbon dioxide peaking just below a mole fraction of 0.8.

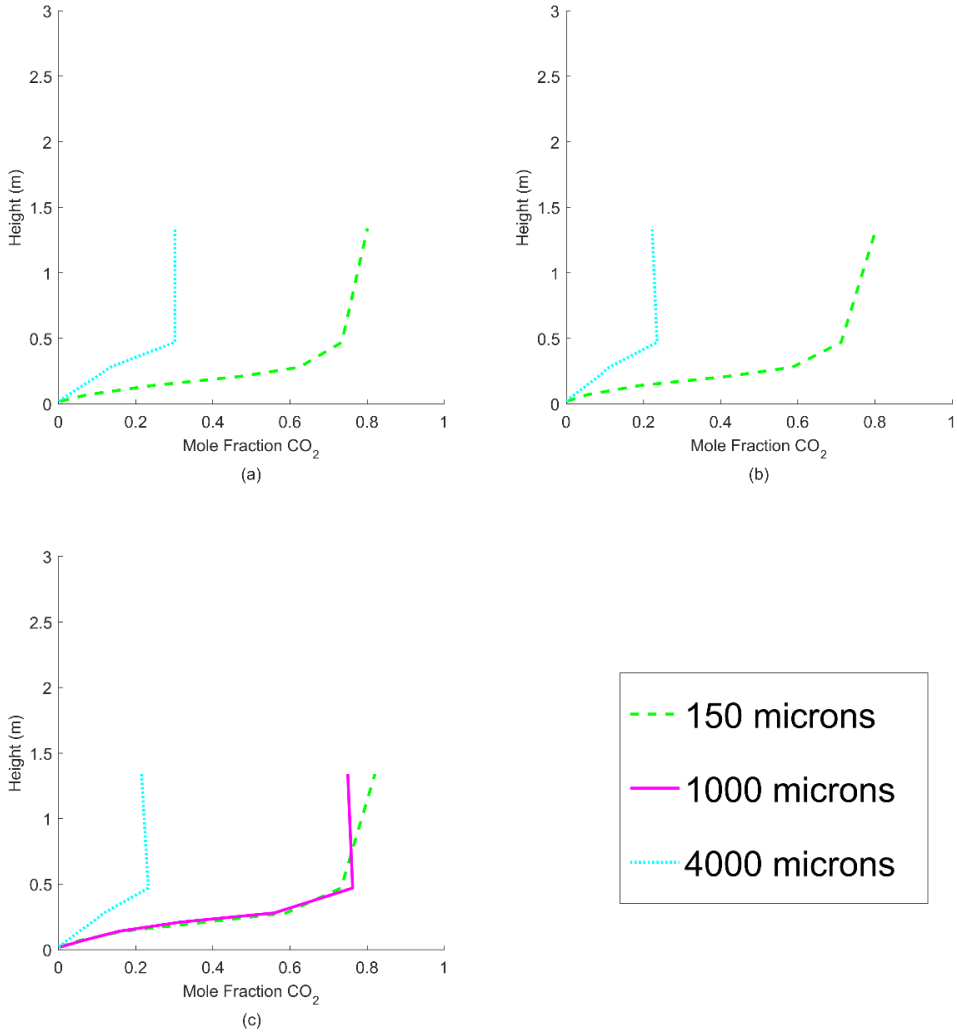

Figure 7: Fuel reactor average carbon dioxide mole fraction effect of coal particle diameter (a) one-step combustion (b) two-step combustion (c) detailed coal char with ash

3.3 Gas Temperature

The gas temperature in the air reactor was very uniform for all cases. The average gas temperature in the dense bubbling bed was 950 °C. The gas temperature increased in the top of the bed and in the riser to about 970 °C. The fuel reactor gas temperatures as an effect of heat input can be found in Figure 8. For the one-step combustion case, the 10 kW coal input temperature results were opposite than expected as more heat input should result in an increase temperature in the gas; however, the 10 kW showed the lowest temperatures. The bottom of the bed the gas heats to the bed temperature of 950 °C and increases to about 975 °C at the top of the dense bed. The temperature then spikes between 1100 °C and 1150 °C. The two-step combustion case corrects as the 20 kW was greater than the 10 kW heat input run, but still the 15 kW heat input temperatures were below the 10 kW. In only the detailed coal case does increasing coal heat input increase the gas temperature as expected. The 10 kW followed a similar temperature profile as the one-step and two-step case. The 15 kW had a higher

temperature through the system and peaked at just below 1250 °C. The 20 kW run had the highest temperatures through the reactor and peaked above 1250 °C.

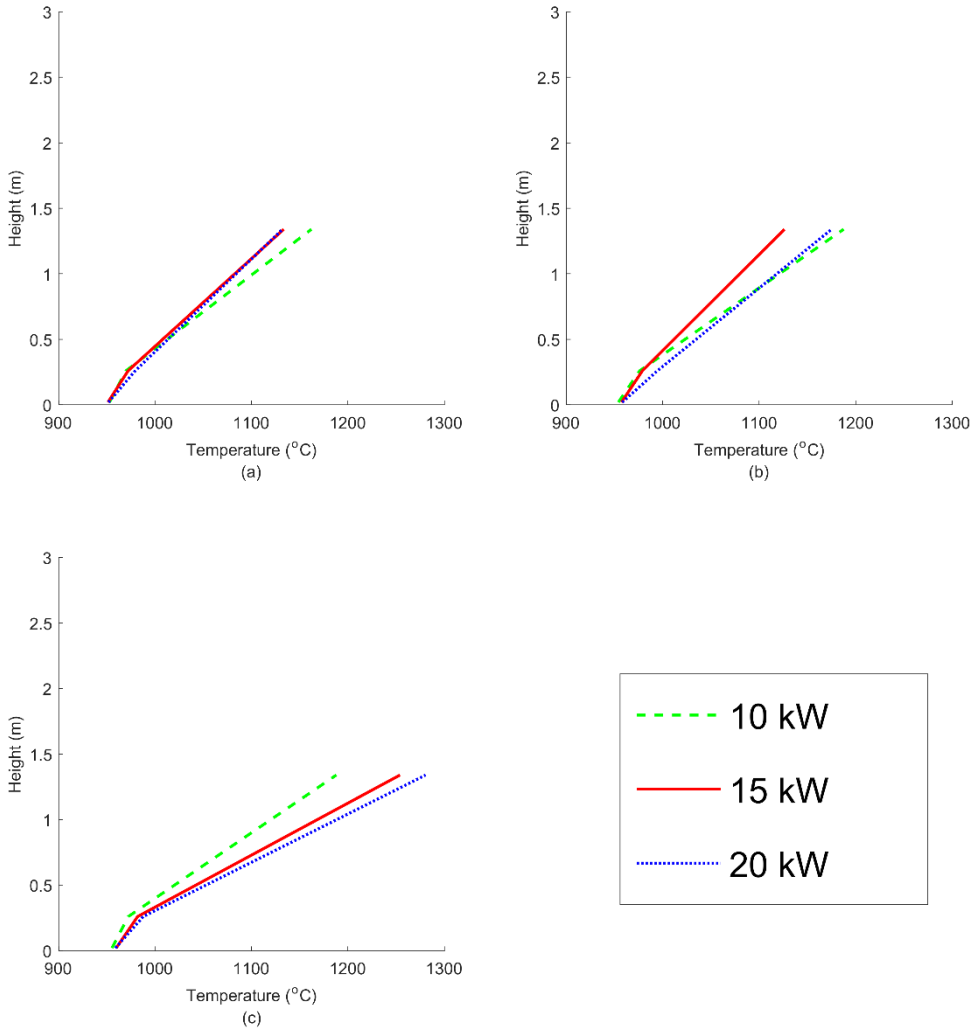

Figure 8: Gas temperature effect of the heat input from coal (a) one-step combustion (b) two-step char combustion (c) detailed coal char with ash

The effects of the particle size on the fuel reactor gas temperature is shown in Figure 9. For all three cases, the 150-micron average diameter PSD runs had the same trends as found in Figure 8, where the temperature increased through the dense bed and then increased dramatically through the dilute phase. The 4000-micron average diameter PSD run was more uniform in temperature throughout the reactor heights at about 950 °C. In the detailed char case, the temperature for the 4000-micron average diameter PSD run slightly dropped due to the endothermic reduction reaction of copper oxide. For the detailed char case, the 1000-micron average diameter PSD run temperature increased through the dense phase and then was constant through the dilute phase due to the low amount of char particles in the dilute phase.

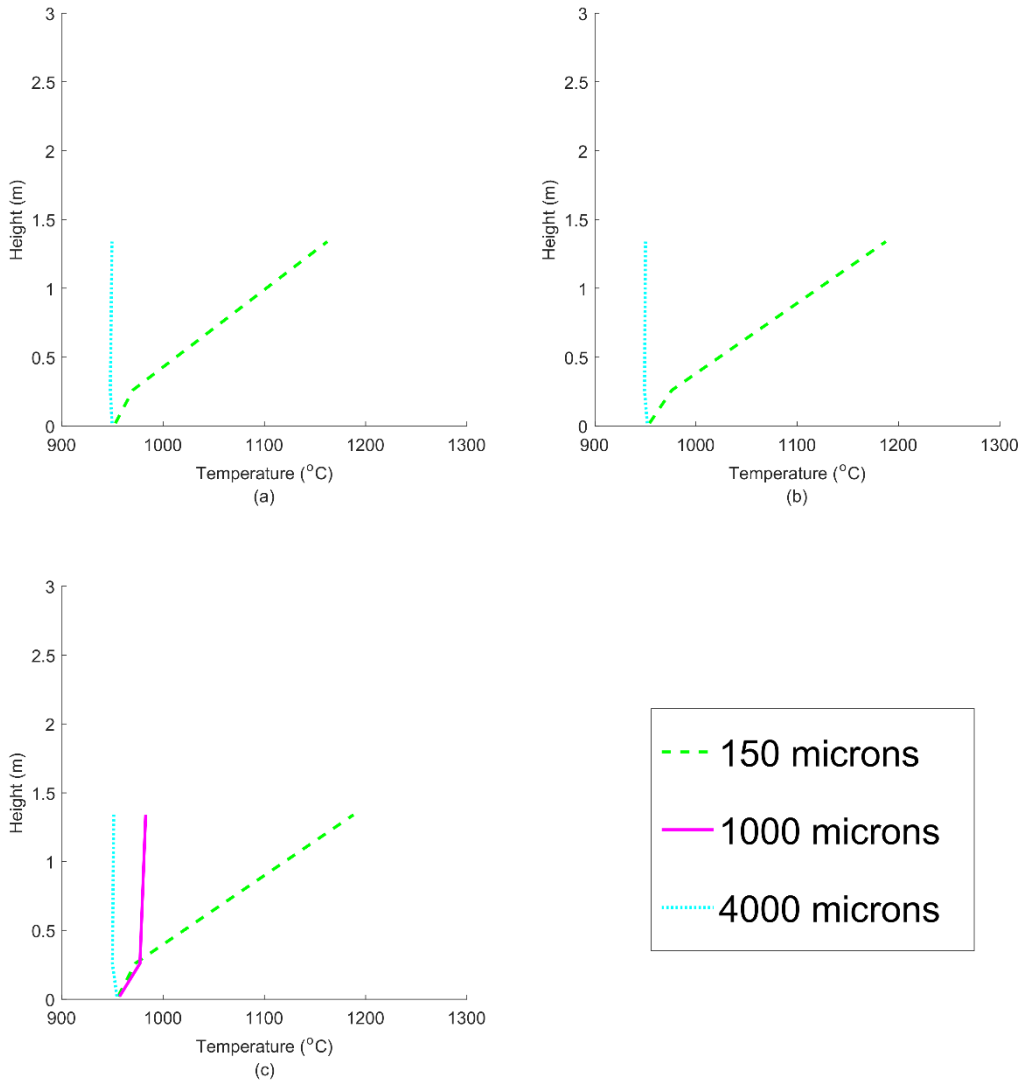

Figure 9: Effect of coal particle diameter on gas temperature (a) one-step combustion (b) two-step char combustion (c) detailed coal char with ash

3.4 Particle Temperature

The particle temperature distribution is shown in Figure 10. For the 150-micron average diameter PSD runs all three cases are similar with a very small mass of particles at temperatures different than the bed temperature of 950 °C. For case one the 4000-micron average diameter PSD run had about 15% of the particles below 800 °C, 20% of the particles below the bed temperature of 950 °C, 50% of the particles were at or below the bed temperature, and 65% of the particles were below 1300 °C. This means that 35% of particles had temperature above 1300 °C. For case two, with the same 4000-micron average diameter PSD, 18% of the particles were below 800 °C, 23% of particles were below 950 °C, 62% were at or below 950 °C, and all particles were below 1250 °C. For case three, 22% of the particles were below 800 °C, 30% of the particles were below 950 °C, 72% of particles were at or below 950 °C, and all particles were below 1125 °C. Only case three had a 1000-micron average diameter PSD run converge.

In this run there were <5% below the 800 °C and 950 °C, 60% at or below the 950 °C bed temperature, 80% were below 1200 °C, and 83% were below 1300 °C.

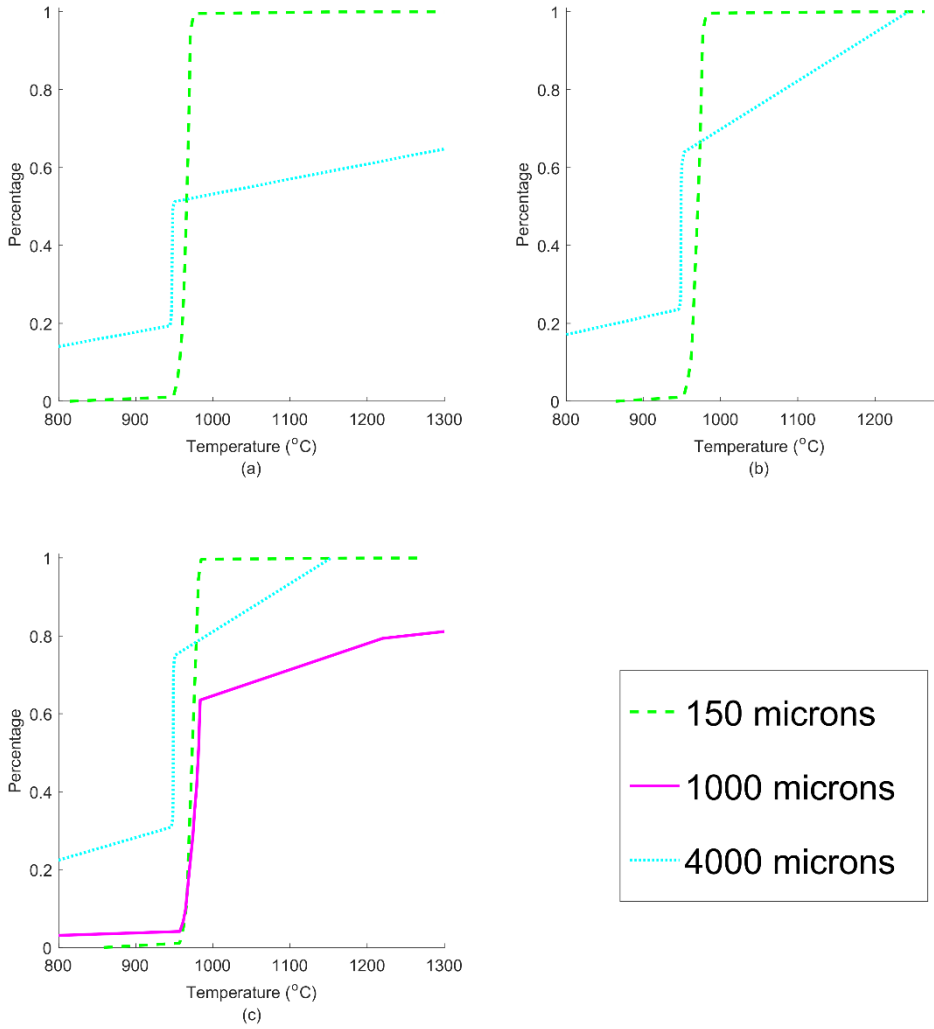

Figure 10: Effect of coal particle diameter on particle temperature distribution in the fuel reactor for (a) one-step combustion (b) two-step combustion (c) detailed coal char with ash

Figure 11 shows the particle temperature distribution in the air reactor. In all cases, the 150-micron and 4000-micron average diameter PSD runs had most temperatures around the bulk bed temperature of 950 °C. The 1000-micron average diameter PSD run, for case three, showed that 95% of particles were at or below 950 °C. The remaining 5% were above this temperature and reached temperatures above 1300 °C.

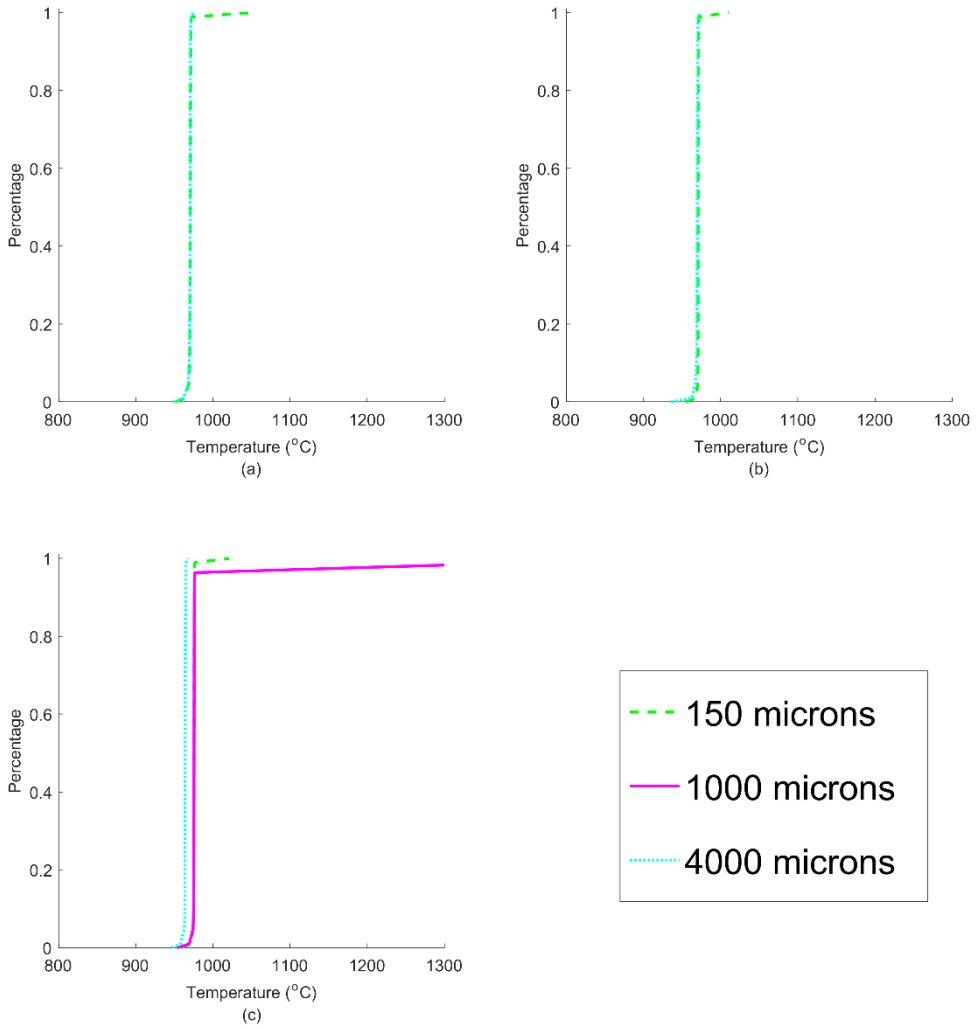

Figure 11: Effect of particle diameter on particle temperature distribution in the air reactor for (a) one-step combustion (b) two-step combustion (c) detailed coal char with ash

4 Conclusion

A bench-scale size unit with a bubbling bed air reactor (AR) and fuel reactor (FR). CLOU copper kinetics were used and the effects of coal parameters and kinetics were explored. With all cases, the 4000-micron average diameter PSD carbon capture efficiency fell below the DOE targeted efficiency of 0.9 after some amount of time. Several of the results suggest that the inclusion of a two-step combustion model and ash constituents in the ash is necessary. For example, for coal particles which were 4000-microns average diameter PSD, steady state was reached more quickly and the temperatures were within a reasonable range. The 1000-micron average diameter PSD case was the most difficult to simulate and only converged when two-step combustion with the detailed char case resulted in completed simulation, albeit, the 1000-micron average diameter PSD case still resulted in excessively high temperatures.

Future work will include gasification reactions to decrease the particle temperatures. Hecht et al. mentions the important of including gasification in oxy-combustion simulations of coal as

there are larger concentrations of carbon dioxide and steam in the reactor [35,36]. However, the FR of a CLOU system contains a high concentration of carbon dioxide and steam, so at the temperatures seen, gasification may be important. Secondly, to also decrease the temperatures of the particles, volatiles will be included in future simulations. This effort will transition some of the heat release from the heterogeneous reactions to homogenous gaseous phase reactions, potentially affecting particle temperature.

5 Acknowledgement

This material is based upon work supported by the University of Wyoming through the Clean Coal Technology Research Fund under grant number 1001541 and by the US Department of Energy (DOE) under award number DE-FE0025076.

All simulation results are the product of Barracuda-VR® licensed from CPFD Software, LLC. This material is based upon work while Dr. Lighty served at the National Science Foundation. Any opinions, findings, and conclusions expressed in this publication are those of the authors and do not necessarily reflect the views of the National Science Foundation.

6 Disclaimer

7 References

[1] IPCC (Intergovernmental Panel on Climate Change), 2013, Climate change 2013: The physical science basis. Working Group I contribution to the IPCC Fifth Assessment Report, Cambridge, United Kingdom: Cambridge University Press.

[2] Metz, B., 2007, Climate change.

[3] United States Environmental Protection Agency, 2012, "Carbon Dioxide Emissions" [Online]. Available: http://www.epa.gov/climatechange/ghgemissions/gases/co2.html.

[4] Stromberg, L., 2001, "Discussion on the potential and cost of different CO2 emission control options," VGB Power Tech.

[5] Granite, E. J., and O'Brien, T., 2005, "Review of novel methods for carbon dioxide separation from flue and fuel gases," Fuel Process. Technol., **86**(14-15), pp. 1423–1434.

[6] Leion, H., Mattisson, T., and Lyngfelt, A., 2009, "Using chemical-looping with oxygen uncoupling (CLOU) for combustion of six different solid fuels," Energy Procedia, **1**(1), pp. 447–453.

[7] Mattisson, T., 2013, "Materials for Chemical-Looping with Oxygen Uncoupling," ISRN Chem. Eng., **2013**(1), pp. 1–19.

[8] Sahir, A. H., Dansie, J. K., Cadore, A. L., and Lighty, J. S., 2014, "A comparative process study of chemical-looping combustion (CLC) and chemical-looping with oxygen uncoupling (CLOU) for solid fuels," Int. J. Greenh. Gas Control, **22**, pp. 237–243.

[9] Markström, P., Linderholm, C., and Lyngfelt, A., 2013, "Chemical-looping combustion of solid fuels - Design and operation of a 100kW unit with bituminous coal," Int. J. Greenh. Gas Control, **15**, pp. 150–162.

[10] Arjmand, M., Keller, M., Leion, H., Mattisson, T., and Lyngfelt, A., 2012, "Oxygen release and oxidation rates of MgAl2O4- supported CuO oxygen carrier for chemical-looping combustion with oxygen uncoupling (CLOU)," Energy and Fuels, **26**(11), pp. 6528–6539.

[11] Sahir, A. H., Sohn, H. Y., Leion, H., and Lighty, J. S., 2012, "Rate analysis of chemical-looping with oxygen uncoupling (CLOU) for solid fuels," Energy and Fuels, **26**(7), pp. 4395–4404.

[12] Ströhle, J., Orth, M., and Epple, B., 2014, "Design and operation of a 1MWth chemical looping plant," Appl. Energy, **113**, pp. 1490–1495.

[13] Lyngfelt, A., 2014, "Chemical-looping combustion of solid fuels – Status of development," Appl. Energy, **113**, pp. 1869–1873.

[14] Jung, J., and Gamwo, I. K., 2008, "Multiphase CFD-based models for chemical looping combustion process: Fuel reactor modeling," Powder Technol., **183**(3), pp. 401–409.

[15] Wang, X., Jin, B., Zhong, W., Zhang, Y., and Song, M., 2011, "Three-dimensional simulation of a coal gas fueled chemical looping combustion process," Int. J. Greenh. Gas Control, **5**(6), pp. 1498–1506.

[16] Wang, S., Lu, H. L., Tang, Y., and Li, D., 2013, "Modeling of a Chemical Looping Combustion Process in Interconnected Fluidized Beds with a Cu-Based Oxygen Carrier," Chem. Eng. Technol., **36**(9), pp. 1503–1510.

[17] Parker, J. M., 2014, "CFD model for the simulation of chemical looping combustion," Powder Technol., **265**, pp. 47–53.

[18] Peltola, P., Ritvanen, J., Tynjälä, T., and Hyppänen, T., 2015, "Fuel reactor modelling in chemical looping with oxygen uncoupling process," Fuel, **147**, pp. 184–194.

[19] Andrews, M., and O'rourke, P., 1996, "The multiphase particle-in-cell (MP-PIC) method for dense particulate flows," Int. J. Multiph. Flow, **22**(2), pp. 379–402.

[20] Snider, D. M., 2001, "An Incompressible Three-Dimensional Multiphase Particle-in-Cell Model for Dense Particle Flows," J. Comput. Phys., **170**(2), pp. 523–549.

[21] O'Rourke, P. J., and Snider, D. M., 2010, "An improved collision damping time for MP-PIC calculations of dense particle flows with applications to polydisperse sedimenting beds and colliding particle jets," Chem. Eng. Sci., **65**(22), pp. 6014–6028.

[22] Sniders, D. M., and O'Rourke, P. J., 2011, "The Multiphase Particle-in-Cell (MP-PIC) Method for Dense Particle Flow," Computational Gas-Solids Flows and Reacting Systems: Theory, Methods and Practice, S. Pannala, M. Syamlal, and T.J. O'Brien, eds., IGI Global, pp. 277–314.

[23] Snider, D. M., Clark, S. M., and O'Rourke, P. J., 2011, "Eulerian–Lagrangian method for three-dimensional thermal reacting flow with application to coal gasifiers," Chem. Eng. Sci., **66**(6), pp. 1285–1295.

[24] Peltola, P., Ritvanen, J., Tynjälä, T., Pröll, T., and Hyppänen, T., 2013, "One-dimensional modelling of chemical looping combustion in dual fluidized bed reactor system," Int. J. Greenh. Gas Control, **16**, pp. 72–82.

[25] Hamilton, M. A., Whitty, K. J., and Lighty, J. S., 2016, "Incorporating Oxygen Uncoupling Kinetics into Computational Fluid Dynamic Simulations of a Chemical Looping System," Energy Technol., **4**(Chemical Looping Technologies), pp. 1–11.

[26] CPFD Software LLC, 2012, "Barracuda Series 15 Training Manual."

[27] Clayton, C. K., Sohn, H. Y., and Whitty, K. J., 2014, "Oxidation Kinetics of Cu 2 O in Oxygen Carriers for Chemical Looping with Oxygen Uncoupling," Ind. Eng. Chem. Res., **53**(8), pp. 2976–2986.

[28] Smoot, L. D., and Smith, P. J., 1985, Fossil Fuel Combustion, New York City.

[29] Yu, J., Zhang, M., and Zhang, J., 2009, "Experimental and numerical investigations on the interactions of volatile flame and char combustion of a coal particle," Proc. Combust. Inst., **32**(2), pp. 2037–2042.

[30] Howard, J. B., Williams, G. C., and Fine, D. H., 1973, "Kinetics of carbon monoxide oxidation in postflame gases," Symp. Combust., **14**(1), pp. 975–986.

[31] Bodryakov, V. Y., 2015, "Specific Heat and Thermal Expansion of Refractory Nonmetal : CaO," Open Sci. J. Mod. Phys., **2**(4), pp. 50–54.

[32] Morrell, R., 2015, "Thermal conductivities," Gen. Phys. (Kaye Laby Tables Phys. Chem. Constants) [Online]. Available: http://www.kayelaby.npl.co.uk/general_physics/2_3/2_3_7.html.

[33] Larsen, R., 2014, "Construction and initial testing of a lab-scale Chemical Looping system," Chalmers University of Technology.

[34] Markström, P., Berguerand, N., and Lyngfelt, A., 2010, "The application of a multistage-bed model for residence-time analysis in chemical-looping combustion of solid fuel," Chem. Eng. Sci., **65**(18), pp. 5055–5066.

[35] Hecht, E. S., Shaddix, C. R., Geier, M., Molina, A., and Haynes, B. S., 2012, "Effect of CO2 and steam gasification reactions on the oxy-combustion of pulverized coal char,"

Combust. Flame, **159**(11), pp. 3437–3447.

[36] Hecht, E. S., Shaddix, C. R., and Lighty, J. S., 2013, "Analysis of the errors associated with typical pulverized coal char combustion modeling assumptions for oxy-fuel combustion," Combust. Flame, **160**(8), pp. 1499–1509.